In-Situ Growth of Metal Oxide Nanoparticles on Cellulose Nanofibrils for Dye Removal and Antimicrobial Applications

Valencia, L.; Kumar, S.; Nomena, E.M.; Salazar-Alvarez, G.; Mathew, A.P.

DOI
10.1021/acsanm.0c01511

Publication date
2020

Document Version
Final published version

Published in
ACS Applied Nano Materials

ACS APPLIED NANO MATERIALS

www.acsanm.org Article

In-Situ Growth of Metal Oxide Nanoparticles on Cellulose Nanofibrils for Dye Removal and Antimicrobial Applications

Luis Valencia,* Sugam Kumar, Emma M. Nomena, German Salazar-Alvarez, and Aji P. Mathew*

Cite This: *ACS Appl. Nano Mater.* 2020, 3, 7172−7181 Read Online

ACCESS | Metrics & More | Article Recommendations | Supporting Information

ABSTRACT: Nanocellulose is known to act as a platform for the in-situ formation of metal oxide nanoparticles, where the multiple components of the resultant hybrids act synergistically toward specific applications. However, typical mineralization reactions require hydrothermal conditions or addition of further reducing agents. Herein, we demonstrate that carboxylated cellulose nanofibril-based films can spontaneously grow functional metal oxide nanoparticles during the adsorption of heavy metal ions from water, without the need of any further chemicals or temperature. Despite the apparent universality of this behavior with different metal ions, this work focuses on studying the in-situ formation of copper oxide nanoparticles on TOCNF films as well as the resultant hybrid films with improved functionality toward dye removal from water and antimicrobial activity. Using a combination of cutting-edge techniques (e.g., in-situ SAXS and QCMD) to systematically follow the nanoparticle formation on the nanocellulosic films in real time, we suggest a plausible mechanism of assembly. Our results confirm that carboxylated cellulose nanofibril films act as universal substrate for the formation of metal oxide nanoparticles, and thus hybrid nanomaterials, during metal ion adsorption processes. This phenomenon enables the upcycling of nanocellulosic materials through multistage applications, thus increasing its sustainability and efficiency in terms of an optimal use of resources.

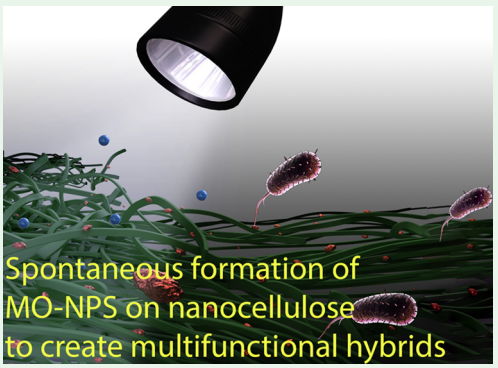

KEYWORDS: *nanocellulose, hybrids, metal oxide nanoparticles, in-situ growth, dye removal, antimicrobial*

INTRODUCTION

Biopolymers are promising building blocks for the preparation of high-performance hybrid materials, especially in terms of efficiency, sustainability, and environmental-friendliness.[1,2] In this context, nanocellulose (NC) has currently been considered as one of the nanomaterials for the future because of the renewability and abundance of its source as well as the fascinating features that NC possesses, such as excellent mechanical properties, low density, and ease of processability into bulk materials.[3−7] NC also offers a versatile surface chemistry that allows to tailor specific properties, for instance, to promote the growth of different nanoparticles (NPS), such as metal−organic frameworks (MOFs),[8] metal (oxide) nanoparticles,[9−14] silica nanoparticles,[15] or carbon nanomaterials.[16] This capability opens multiple opportunities toward the design of hybrids for diverse applications. One of the most promising and widely studied hybridizations of NC is the mineralization of transition metal oxide nanoparticles (MO-NPS)—an important class of semiconductors with applications in adsorption, energy, electronics, gas sensors, and catalysis. Nevertheless, the in-situ growth of MO-NPS on NC is typically achieved via chemical reduction methods[12] or under hydrothermal conditions[17] for which the use of toxic chemicals and high energy consumption are subjects of concern.

The TEMPO-mediated oxidation of cellulose nanofibrils (CNF) (to form TEMPO-oxidized cellulose nanofibrils, TOCNF) has opened a wide window of opportunities for the utilization of CNF in various applications, including adsorption of metal ions, charged dyes, radioactive species,[18] and viruses.[19−22] Moreover, TOCNF, due to their strong interfibril connections, high aspect ratio, and high degree of defibrillation, offer the possibility to create robust nanomaterials via different processing techniques such as casting/vacuum filtration to prepare 2D films. Previously, in our research group, we have observed the formation of metal oxide aggregates (around 0.3−1 μm) on the surface of TOCNF films upon adsorption of metal ions from their aqueous solutions,[23−25] suggesting a preformation of smaller NPS that had coalesced and aggregated to form those larger aggregates. However, the mechanism of how such NPS form, together with their functionality, has not yet been understood.

Received: June 2, 2020
Accepted: June 4, 2020
Published: June 4, 2020

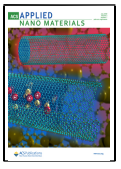

https://dx.doi.org/10.1021/acsanm.0c01511
ACS Appl. Nano Mater. 2020, 3, 7172−7181

Herein, we mechanistically demonstrate the ability of TOCNF films to spontaneously grow MO-NPS during the adsorption of metal ions from aqueous solutions, at room temperature conditions and without addition of any reducing agent. Most part of the article is destined to study the adsorption of copper ions (Cu^{2+}) onto TOCNF films to understand the subsequent growth of copper oxide nanoparticles (Cu_2O-NPS). However, many of the critical results obtained here for Cu^{2+} are also verified for silver (Ag^{+}) and iron (Fe^{3+}) ion solutions, proving the universality of the phenomena. The Cu_2O-NPS are formed within TOCNF while interacting with copper salt ($Cu(NO_3)_2$) solutions of different concentrations. We first show the existence of the formed Cu_2O-NPS via X-ray scattering as well as microscopic and spectroscopic techniques. Then, we studied their assembly and formation by combining different in-situ techniques. The resultant hybrid (hereafter denoted as Cu_2O/TOCNF) films exhibit the functionality of the Cu_2O-NPS for enhanced dye removal from water and antimicrobial properties, proving the ease of preparation of multifunctional hybrid materials upon simply adsorption of metal ions. This study introduces the concept of a multistage employment of nanocellulose via upcycling the materials after use. Such a versatile and energy-efficient way to introduce functionality to bio-based materials establishes a strong and sustainable pathway that can be extended toward different applications.

EXPERIMENTAL PART

Chemicals and Materials. High-purity cellulose from softwood fibers (Norwegian spruce) with high cellulose content (95% cellulose, 4.5% hemicellulose, and 0.1% lignin content as provided by Domsjö Fabriker AB, Sweden) was used as starting material to produce TOCNF. (2,2,6,6-Tetramethylpiperidin-1-yl)oxyl (TEMPO), sodium bromide (NaBr), sodium hypochlorite (NaClO), copper nitrate ($Cu(NO_3)_2$), silver nitrate $Ag(NO_3)$, iron(III) nitrate nonahydrate ($Fe(NO_3)_3{\cdot}9H_2O$), methylene blue (MB), and (3-aminopropyl)-triethoxylsilane (APTES) were purchased from Sigma-Aldrich and used as received. Cellulose nanofibril suspensions (1.8 wt % in water) were employed for the preparation of the membranes for the in-situ SAXS measurements, and they were acquired from Borregard, Norway, as the commercial product Exilva.

Fabrication of TEMPO-Oxidized Cellulose Nanofibrils. TOCNF was obtained from a defibrillation process of soft wood pulp. In brief, an aqueous suspension of pulp from Norwegian spruce was subjected to TEMPO-mediated oxidation using TEMPO, NaClO, and NaBr following the conventional procedure proposed by Isogai et al.[19,26] The resultant carboxylated cellulose suspension (1.2 mmol/g_{TOCNF}) was subjected to mechanical disintegration using a high-pressure homogenizer to yield fully defibrillated TOCNF. For the grinding, a 0.5 wt % suspension was passed through the homogenizer five times at a pressure of 500 bar.

Preparation of TOCNF Films. TOCNF films (thickness ≈10 μm) were prepared by pouring TOCNF suspension (40 g, 0.5 wt % in water) into plastic Petri dishes after degassing to remove any presence of bubbles and dried in an oven at 35 °C (pressure = 1 bar) for 24 h.

Characterization. *Microscopy.* The size of the nanoclusters and surface topography of the TOCNF films before and after metal ion adsorption were examined by atomic force microscopy (AFM) utilizing a Nanoscope V (Veeco Instruments, Santa Barbara, CA) in tapping mode. All images were analyzed by using Scanning Probe Image Processor (SPIP) software. Scanning electron microscopy (SEM) micrographs of the films were acquired in a JEOL 7000 with accelerated voltage of 2 kV. The specimens were coated with a thin gold layer prior visualization.

Spectroscopy. The chemical structure of the hybrid films was characterized via X-ray photoelectron spectroscopy (XPS). The analyses were performed with an Axis Ultra DLD electron spectrometer (Kratos Analytical Ltd., U.K.) using a monochromatized A1 Kα radiation source operating at 150 W and an energy of 20 eV for individual photoelectron lines. The high-resolution spectra were fitted by using a series of Gaussian peaks. UV−vis spectroscopy measurements were performed using a Thermo Scientific GENESYS UV−vis spectrophotometer using quartz cuvettes.

X-ray Diffraction. The crystalline structure of the in-situ growth Cu_2O-NPS on TOCNF films was studied by using powder X-ray diffraction (PXRD). The experiments were performed by using a PANalytical X'Pert PRO X-ray system with the following settings: current 40 mA, tension of 45 kV, at a temperature of 25 °C with step size (2θ) of 0.05. The diffracted intensity of Cu Kα radiation (wavelength of 0.154 nm) was recorded in the scattering angle range from 20° to 65° in reflection mode. For the measurements, a TOCNF film was submerged into a $Cu(NO_3)_2$ aqueous solution (800 mg L^{-1}) for 60 min and dried at room temperature conditions overnight.

Quartz-Crystal Microbalance with Dissipation (QCMD). The adsorption of Cu^{2+} ions on TOCNF was investigated by QMCD using the Insplorion Acoulyte (Insplorion AB, Göteborg, Sweden, www.insplorion.com) attached to the QCMD E1 system, Q-Sense AB, using SiO_2 sensors. TOCNF was deposited on cleaned sensors (cleaned by UV/ozone for 20 min and rinsed with water) from a TOCNF aqueous suspension (0.2 wt %) using spin-coating (SPIN150i) at 2500 rpm for 2 min. Prior to the deposition of TOCNF, the sensors were exposed to APTES for 2 min, which eventually act as an anchor to stably deposit the nanofibers onto the sensors. These sensors were then installed in the flow cell, and water was allowed to flow at a rate of 0.200 mL min^{-1} for at least 1 h until a stable baseline was obtained; then the water was replaced with $Cu(NO_3)_2$ aqueous solutions of variable concentration.

The adsorbed mass was calculated by using the Sauerbrey equation. The size of the intermediate nanoclusters was approximated from the QCMD data by utilizing the conventional Sauerbrey model and the model proposed by Tellechea et al.[27] In the Sauerbrey method, it is assumed that the ion adsorption results in the formation of a homogeneous film on the sensor where the thickness (Sauerbrey thickness) of the film can be calculated by dividing the Sauerbrey mass ($\Delta m_{Sauerbrey}$) by the density of the material. This Sauerbrey thickness can be correlated to the size of the small nanoclusters formed in the cellulose due to the ion adsorption. Though this is not an exact method, it can provide a rough estimate of the nanocluster size. The method proposed by Tellechea et al., on the other hand, is used for the studies where the adsorption on the QCMD sensor takes place in the form of the discrete particles (details of the calculations are further described in the Supporting Information). Even though the present system under study is somewhere in between the two extremes (i.e., formation of the completely homogeneous film or deposition of the discrete particles), the calculations performed by using both the methods reveal the existence of the small nanoclusters at the beginning (roughly about 30 min, after replacing the water by salt solution).

Synchrotron-Based Small-Angle X-ray Scattering (SAXS). The measurements were performed by passing the metal solutions (100 mg/L) through (by applying vacuum through the output of the setup) a film (50 mm diameter, hermetically sealed by O-rings) mounted perpendicularly to the X-ray beam. The films for the measurements were prepared as follows: First, a substrate was prepared by vacuum filtration of 1 wt % suspension of CNF using a Buchner funnel setup having an area of 143 cm^2, resulting in a homogeneous membrane with grammage of 20 g/m^2. Then, a thin layer of TOCNF (grammage of 0.4 g/m^2) was deposited over the substrate also by vacuum filtration. The membranes were dried at room temperature for 2 days under a load of 5 kg after each step. The thickness of the membranes was determined by using SEM to be 19.3 μm. It is worth to mention that the employment of a CNF substrate was essential for these experiments, since pure TOCNF films were not strong enough to withstand the vacuum pressure and water flux at which the films were submitted. Moreover, pristine CNF does not exhibit any functionality other than hydroxyl groups and therefore is considered to not significantly influence the results here attributed to TOCNF.

The measurements were performed at the micro- and nanofocus X-ray scattering (MiNaXS) beamline P03 at synchrotron source PETRA

https://dx.doi.org/10.1021/acsanm.0c01511
ACS Appl. Nano Mater. 2020, 3, 7172−7181

III, DESY, Germany. A beam of X-rays having wavelength (λ) of 0.09 nm and size of 20 × 20 μm^2 is made incident on the samples while the scattered X-rays were detected by using a 2D-pixel detector (Pilatus 300K). The scattering intensity $I(Q)$ is radially averaged for different scattering vectors Q ($Q = ((4\pi \sin(\theta))/\lambda)$, where 2θ is the scattering angle). The sample-to-detector distance was 1.5 m, and the transmission of the X-rays across the films was monitored simultaneously by a PIN diode during the scanning experiment. The homogeneity of the samples and reproducibility of the scattering data were confirmed by acquiring the data in repeated scan at five different sample positions.

In SAXS, the scattering intensity as a function of scattering vector (Q) can be expressed as

$$I(Q) = nP(Q)S(Q) \quad (1)$$

where n is a Q-independent term which is proportional to the volume fraction of the scatterers in the scattering volume and the scattering contrast. $P(Q)$ denotes the intraparticle structure factor (form factor) which is decided by the shape and the size of the particles. $S(Q)$ represents the interparticle structure factor which provides interparticle interaction between the particles. In the absence of strong interparticle correlations (e.g., in the case of a dilute system), $S(Q)$ may be approximated to unity.

For a spherical particle having radius R, $P(Q)$ can be given as

$$P(Q) = \left[3\frac{\sin(QR) - (QR)\cos(QR)}{(QR)^3}\right]^2 \quad (2)$$

For the polydispersed system, the $P(Q)$ can be convoluted with a size distribution function, as follows:

$$P(Q) = \int P(Q, R) f(R)\, dR \quad (3)$$

where $f(R)$ is the size distribution and can be accounted by the log-normal distribution, as expressed by

$$f(R) = \frac{1}{R\sigma\sqrt{2\pi}} \exp\left[-\frac{\left(\ln\frac{R}{R_{med}}\right)^2}{2\sigma^2}\right] \quad (4)$$

where R_{med} and σ are the median value and the standard deviation, respectively. The mean (R_m) and median values (R_{med}) are related as $R_m = R_{med} \exp(\sigma^2/2)$.

For some nonparticulate and randomly distributed two-phase systems (like the dry films in the present system), the SAXS intensity can be modeled by the following generalized Debye–Anderson–Brumberger (gDAB) equation:

$$I = \frac{I_0}{(1 + Q^2\xi^2)^\alpha} \quad (5)$$

where α is the exponent and ξ represents the correlation length, providing a measure of the average spacing between regions of phase 1 and phase 2.

Applications of in-Situ Grown MO-NPS. *Dye Removal from Aqueous Solutions.* To examine the dye removal capacity of the resultant hybrid films, MB was chosen as a probe molecule: 7 mL of MB was added into glass vials containing TOCNF or Cu_2O/TOCNF films (prepared by submerging a TOCNF film in a $Cu(NO_3)_2$ solution (800 mg/L) for 60 min and drying overnight at room temperature), respectively (around 90 mg). Then, the reaction mixture was kept under UV–vis light to initiate the reaction, and the distance between the light source and the reaction mixture was fixed at 10 cm. The UV light was provided by a UV lamp with major emission at lambda 365 nm (6 W). At a regular irradiation time, the dye containing solution was quantified by measuring the absorbance using UV–vis spectroscopy. The efficiency of dye removal was calculated via eq 6, where A_0 is the initial absorbance of the dye and A_t is the absorbance at a specific time.

$$\%\ \text{dye removal} = \frac{A_0 - A_t}{A_0} \times 100 \quad (6)$$

Antimicrobial Activity. The antimicrobial activity of the films was assessed by using two types of common pathogens: a Gram-negative one (*Escherichia coli* K12) and a Gram-positive one (*Listeria innocua* ATCC 33090). For the tests, exponentially growing cultures of the strains were diluted to approximately 200 cells/mL. Diluted cultures were placed on the films inside of polystyrene cell culture wells and incubated without stirring for 24 h at 37 °C. The films were then carefully washed with distilled water to remove planktonic and loosely attached cells. The visualization of the bacterial cells was performed by confocal microscopy, 24 h after inoculation using a Leica TCS-SP5 and DMI6000 inverted microscope (Leica GmbH, Germany). Viable and nonviable bacteria were tracked using the Live/Dead BacLight Bacterial Viability Kit (Sigma-Aldrich). For staining, the surface of each specimen was covered with 100 μL of stain (a 2:1 mixture of calcein AM and propidium iodide in buffer solution) and then incubated at 37 °C for 15 min prior imaging. Calcein AM stains viable cells only (excitation: 488 nm; emission: 500–530 nm), while propidium iodide stains dead cells (excitation: 488 nm; emission 600–630 nm). Films without nanoparticles were used as references.

RESULTS AND DISCUSSION

The mineralization of MO-NPS on cellulosic films typically requires hydrothermal conditions or reducing agents. Nevertheless, we have observed in our previous works[23−25] that carboxylated nanocellulose films (TOCNFs) can in situ grow metal oxide aggregates during the adsorption of metal ions from aqueous solutions at room temperature, which suggests a preformation of NPS that had coalesced and aggregated. In this work, we mechanistically study the ability of TOCNF films to spontaneously grow MO-NPS during metal ion adsorption processes (see Figure 1). Although this seem to be a universal behavior, most of this study is destined to study the adsorption of Cu^{2+} ions onto TOCNF films to subsequently grow Cu_2O-NPS as well as the gained functionality of the films upon hybridization.

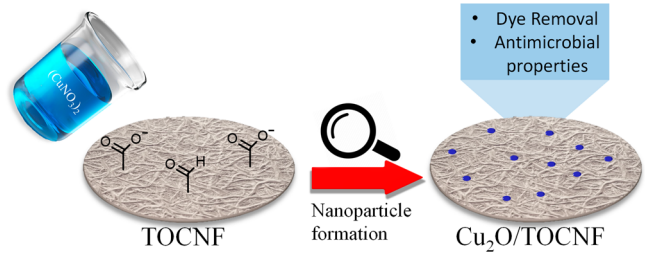

Figure 1. Conceptual schematic illustration displaying the in-situ growth of Cu_2O-NPS on TOCNF films to form Cu_2O/TOCNF hybrid films with dye removal and antimicrobial properties.

Figure 2 shows the characterization of the Cu_2O-NPS formed on the TOCNF films, resulting from the interaction between the carboxylate groups and Cu^{2+} ions. For the AFM analysis, the TOCNF films were dipped in $Cu(NO_3)_2$ solutions of variable concentrations (100, 200, 400, and 800 mg L^{-1}) for ~1 h, rinsed, and dried. The results, shown in Figure 2a,b, reveal the presence of the Cu_2O-NPS embedded on the surface of the films, denominated upon hybridization as Cu_2O/TOCNF. The NPS exhibit an irregular shape and a mean diameter of about 26 nm (Figure S1). In addition, larger aggregates of size >100 nm can also be observed via SEM (Figure S2). The presence of Cu_2O-NPS was furthermore corroborated by PXRD (Figure 2c).

The resultant pattern displays the appearance of small diffraction peaks around 35° and 60°, indicating that the formed NPS correspond to cuprous oxide (Cu_2O) exhibiting (111) and

https://dx.doi.org/10.1021/acsanm.0c01511
ACS Appl. Nano Mater. 2020, 3, 7172−7181

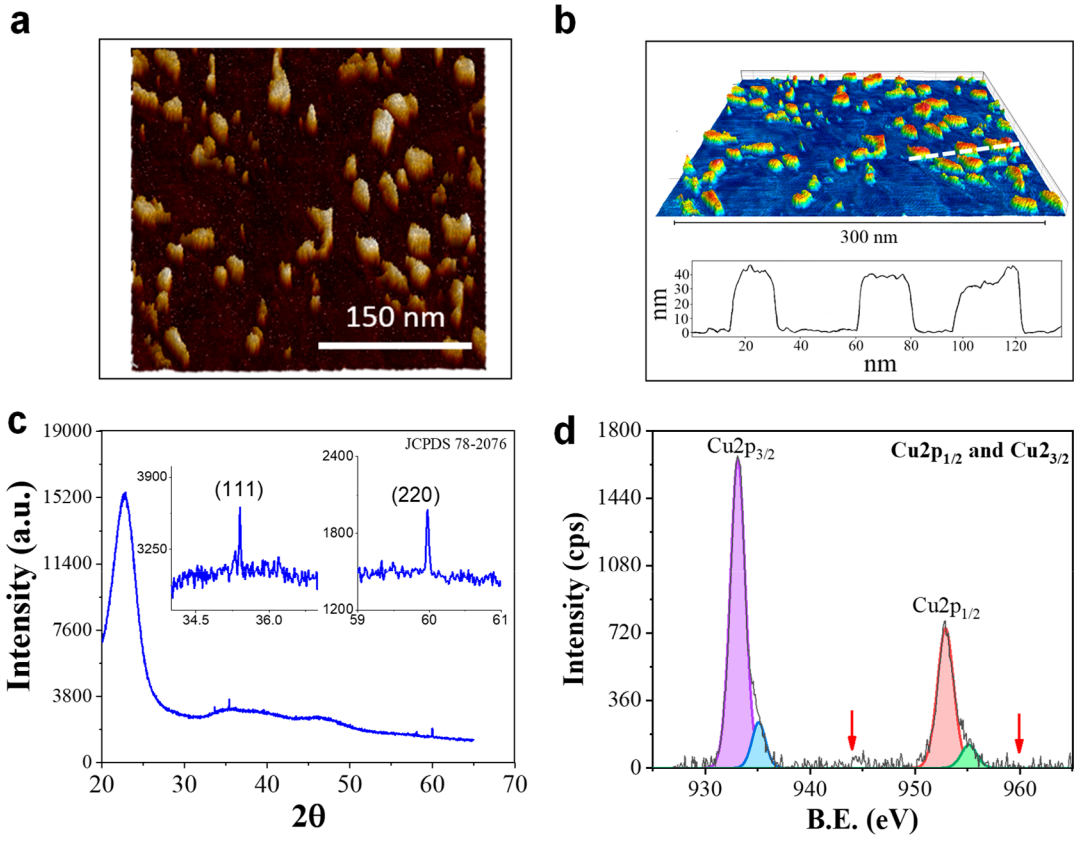

Figure 2. Morphological analysis of in-situ growth Cu_2O-NPS. (a, b) Surface topography of the TOCNF film after adsorption of metal ions studied by AFM (phase images) revealing the formation of NPS with a mean diameter of 26 nm. (c) XRD pattern revealing the crystalline phase of the Cu_2O-NPS. (d) High-resolution Cu $2p_3$ XPS spectra of the Cu_2O/TOCNF hybrid film.

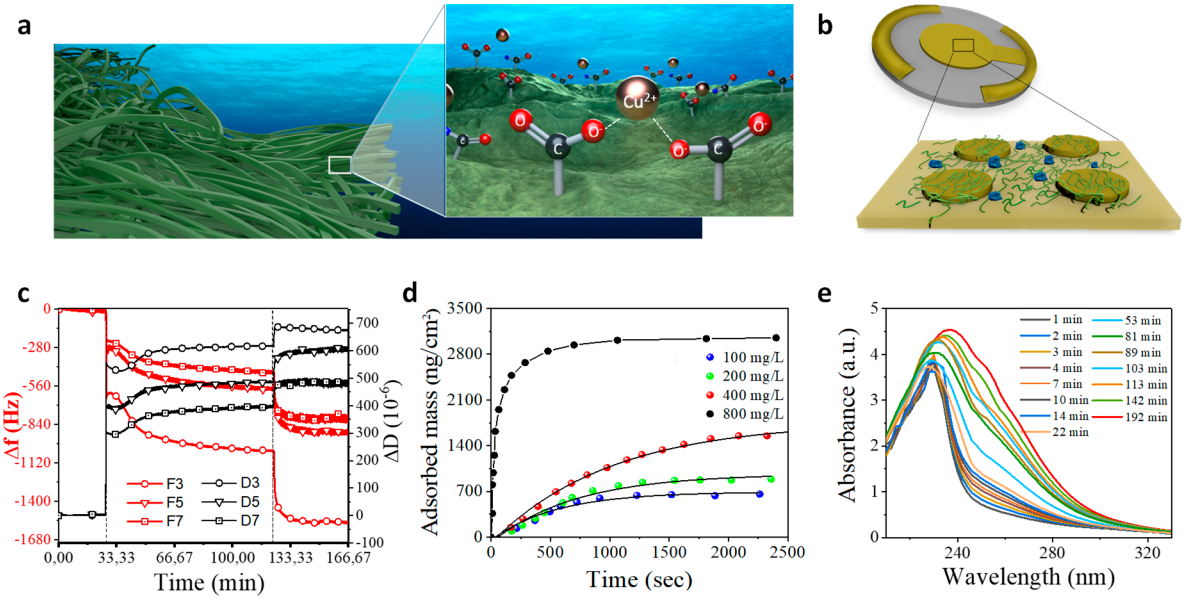

Figure 3. Adsorption studies using QCMD and UV−vis spectroscopy. Schematic illustration of (a) the adsorption of metal ions on TOCNF and (b) the TOCNF coating a QCMD sensor and the subsequent Cu_2O-NPS formation. (c) QCMD studies of copper adsorption (800 mg L^{-1}, as a representative concentration). (d) Variation of the adsorbed mass with increasing time, for different concentrations of Cu^{2+} metal ion solutions as determined by the Sauerbrey equation, employing third overtone. (e) UV−vis spectra of TOCNF film tracking the formation of Cu_2O nanoclusters (400 mg L^{-1} $Cu[NO_3]_2$).

(220) planes of the standard cubic cuprite structure of copper[28] [JCPDS file No. 05-0667]. However, the Cu_2O diffraction peaks were in great extent overshadowed by the broad predominant peaks corresponding to the cellulose I polymorph (pristine TOCNF spectra shown in Figure S3): 22.67° (200) and and 34.5° (040).[29] The oxidation state of the Cu_2O-NPS was

https://dx.doi.org/10.1021/acsanm.0c01511
ACS Appl. Nano Mater. 2020, 3, 7172−7181

confirmed via high-resolution Cu_2p_3 XPS spectra (Figure 2d), where two sharp peaks observed at 934.5 and 954.5 eV can be attributed to Cu $2p_{3/2}$ and $2p_{1/2}$, respectively.[30] The oxidation state corresponding to Cu(I) oxide is demonstrated by the almost undistinguishable satellite features of Cu 2p, as typically Cu(II) exhibits very prominent signals at 943 eV (marked with red arrows). It is worth mentioning that the variation of some experimental protocols may influence the nature of the formed NPS, whereas the exact dependency is still required to be established.

Mechanism of the Nanoparticle Formation. The growth of the Cu_2O-NPS was systematically studied in real time by combining the use of different ultrasensitive in-situ techniques including SAXS, QCMD, and UV−vis spectroscopy. Following the growth and coalescence model, we propose a possible mechanism of nanoparticle formation consisting of mainly three parts: (i) adsorption of the metal ions onto carboxyl groups, (ii) reduction of metal atoms and growth of nanoclusters, and (iii) coalescence and formation of NPS. Each stage of the mechanism is discussed in the following sections.

Adsorption of Metal Ions. The negatively charged carboxyl groups of TOCNF are known to interact with metal ions[31] (Figure 3a), acting as anchor groups via the formation of electrostatic interactions and covalent bonding, as calculated by Williams et al.,[32] who reported that transition metal cations undertake stronger covalent bonds with TOCNF, as opposed to alkali metals where the electrostatic interactions dominate. The real-time adsorption of Cu^{2+} ions on TOCNF was further studied via QCMD, and the results are shown in Figure 3. The QCMD is a nanomechanical acoustic-based technique utilizing an electromechanical sensor to in situ detect exceedingly small changes (of the order of ng/cm^2) in the mass at surfaces in real time. In this technique, a piezoelectric quartz sensor crystal, sandwiched between a pair of electrodes, is excited by the applied AC field to undergo a mechanical shear oscillation, at the resonance frequency, where $f3$, $f5$, $f7$, etc. are the overtone frequencies. In the case, if there is any adsorption of mass on the sensor, the frequency of the oscillation changes and the changes in the frequency are directly proportional to the adsorbed mass, according to the Sauerbrey relation (eq 1 in the Supporting Information). The deposition/loss of mass on/from sensor surface causes a decrease/increase in the resonance frequency. The other parameter which is measured in QCMD is the dissipation factor ($D_n = 2\Gamma_n/f_n$), associated with the dissipative energy losses, as induced by the deposited masses. The change in the dissipation factor provides information about the structural changes and particularly useful when the mass deposition does not occur in the form of rigid and uniform film. Further details on QCMD parameters and data analysis can be found in the Supporting Information.

For the measurements, a homogeneous layer of TOCNF was spin-coated on a QCMD sensor (Figure S4). During the experiment, a flow cell was initially filled with water, waiting until reaching an equilibrium, to then change to solution with a given concentration of Cu^{2+} ions. The frequency shift and the dissipation factor were recorded vs time. Three distinct stages are identified in frequency variation (opposite trends in dissipation factor): first, (i) the sensor in dry conditions, (ii) a frequency decrease upon addition of water due to water adsorption and resultant swelling of the nanofibrils followed by stabilization, and finally (iii) a sharp further decrease in the frequency upon addition of the copper solution (Figure 3b) indicating the rapid adsorption of the Cu^{2+} ions onto the cellulose nanofibrils.

As the frequency shift is directly proportional to the adsorbed mass onto the TOCNF, the adsorbed Cu^{2+} ions can be calculated (via the Sauerbrey equation), which are found to vary as a function of metal ion concentration in the solution (Figure 3c). The saturation value, i.e., the final adsorbed mass, increases linearly as a function of metal ion concentration because of the shifting equilibrium existing between the ions and the functional carboxyl groups of TOCNF (see Figure S5). It is indeed well known that the adsorption capacity increases as a function of initial concentration of the sorbate (in this case Cu^{2+} ions), as reported in several other research works.[33−35] This behavior is expected to be followed until establishing an equilibrium, where no available functional groups can accommodate sorbate molecules. In that case, further increment in initial concentration of sorbate would not significantly influence the adsorption capacity. Because equilibrium is not attained for the salt ion concentrations under investigations, it is expected that all Cu^{2+} are adsorbed on the TOCNF film.

Growth of Nanoclusters. A possible explanation of how the adsorbed Cu^{2+} ions can convert into nanoclusters is by reduction through the aldehyde groups present in TOCNF (also formed during the TEMPO-mediated oxidation step of cellulose),[19] which have considerable reduction capabilities, to reduce copper cations from divalent oxidation state to the metallic form. The reaction between an aldehyde and copper ions is very well known, although it typically requires elevated temperatures. This behavior suggests that the anchoring of the metal ions through the carboxyl groups of TOCNF could significantly promote the reduction reaction. The potential of NC to catalyze chemical reactions has been previously reported for other systems.[36,37]

Upon reduction, the high concentration of metal monomers in the solution leads to coalescence and oxidation, as due to their instability metal monomers tend to bind other metal atoms forming higher-mers, leading to nanoclusters. This behavior was corroborated via UV−vis spectroscopy (Figure 3d) of a TOCNF film during adsorption of Cu^{2+} ions, where a spectral feature gradually formed in the wavelength range of 240 nm. The UV absorbance exponentially increases as a function of time (see Figure S6), suggesting the continuous growth of the nanoclusters. Moreover, the appearance of a shoulder at longer wavelengths (≈260 nm) furthermore reveals the growth of the nanoclusters and their increase in population. Upon drying the film, the peak shifts to even longer wavelengths, clearly displaying multiple populations that can be deconvoluted by using various Gaussian distributions (Figure S7), suggesting the growth of Cu_2O-NPS.

The size of the nanoclusters was estimated from the QCMD measurements and found to be in the range about 2−5 nm as approximated to the Sauerbrey thickness (see Table S1) and as calculated from the model proposed by Tellechea et al.[27] (Further details are described in Experimental Part and the Supporting Information.) It should be emphasized here that both approaches may not be exactly applicable in the present case but can be used to get a rough estimate of the nanoclusters size. To follow the in-situ growth of the nanoclusters, SAXS measurements were further performed and discussed later in the article. The SAXS data analysis also suggests the evolution of length scales in the range of 4−6 nm during adsorption of the Cu^{2+} ions (Figure S8).

https://dx.doi.org/10.1021/acsanm.0c01511
ACS Appl. Nano Mater. 2020, 3, 7172−7181

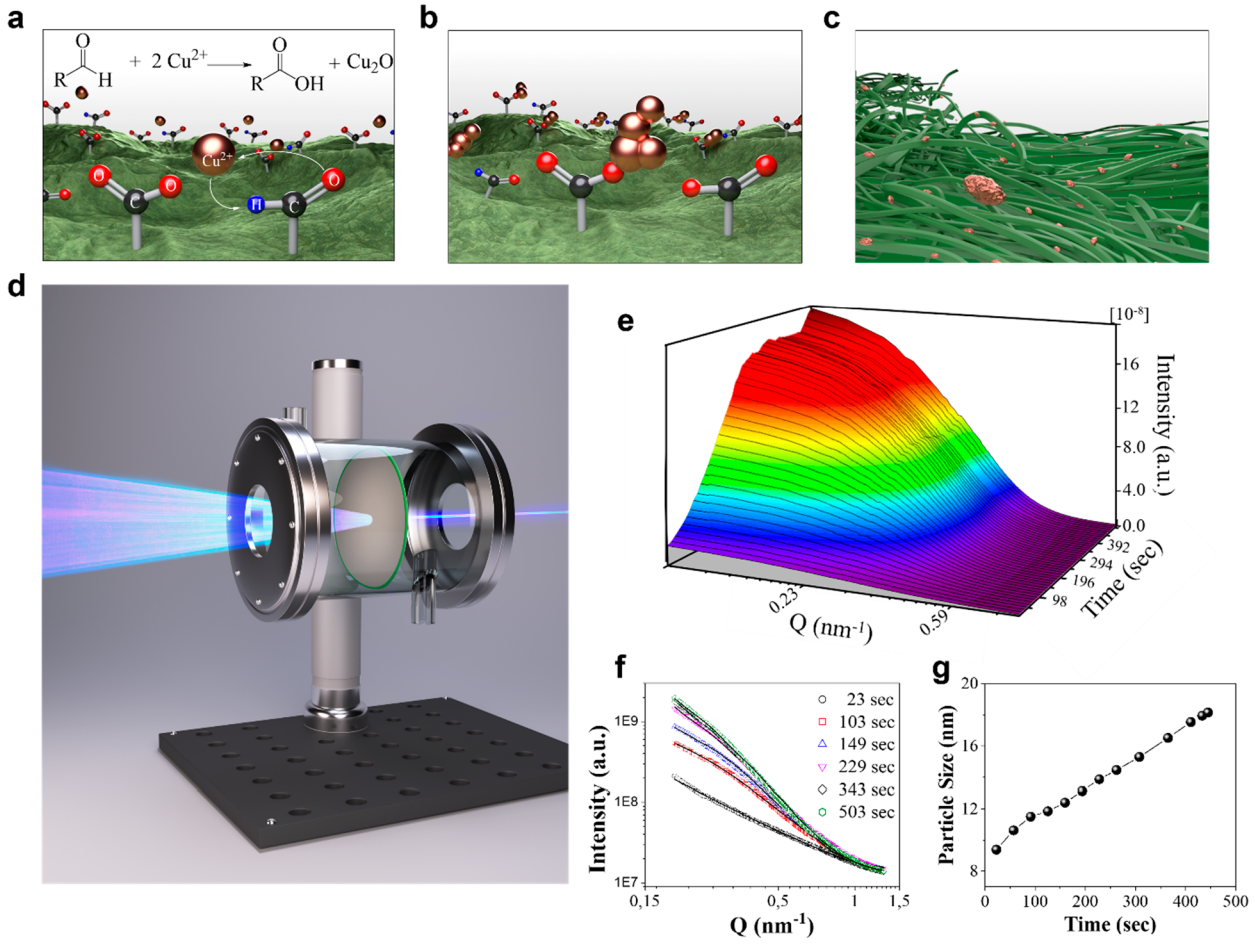

Figure 4. Growth of Cu_2O-NPS on TOCNF. (a–c) Schematic representation of the growth of Cu_2O-NPS on TOCNF. (a) Reduction of Cu^{2+} ions to Cu^{+} by aldehyde groups on TOCNF (becoming carboxyl groups upon reduction). (b) Growth of copper oxide nanoclusters and (c) subsequent coalescence of these nanoclusters forming Cu_2O-NPS. (d–g) In-situ SAXS measurements: (d) Schematic representation of the experimental setup used for the SAXS measurements. (e) Three-dimensional plots [$I(Q)$ vs Q vs time] and (f) two-dimensional [$I(Q)$ vs Q] plots during drying of nanocellulose films after copper adsorption. (g) Size evolution of the Cu_2O-NPS during drying in terms of diameter.

Coalescence and Growth of Nanoparticles. The nanoclusters, formed upon reduction of Cu^{2+} ions (Figure 4a,b), rapidly oxidize and self-aggregate (Figure 4c) via van der Waals or electrostatic forces mainly,[38] to then crystallize and form primarily Cu_2O-NPS. This suggests that TOCNF can stabilize the nanoparticles from subsequent oxidation to Cu(I), but also partially preventing their coagulation to larger aggregates. Although large aggregates can indeed also be observed by SEM microscopy (Figure S2), they are in fact the particles (>100 nm) previously observed in our research group.[34]

The growth of the Cu_2O-NPS in the films was studied in real time via synchrotron-based SAXS experiments, tracking the structural transformations during adsorption of Cu^{2+} ions from $Cu(NO_3)_2$ solution (100 mg L^{-1}). For the measurements a custom-built low-vacuum filtration cell was utilized as reported in our previous work[7,39] (Figure 4d).The $Cu(NO_3)_2$ solution was vacuum filtered through the cellulosic films, while shooting the X-rays perpendicularly.

The SAXS data were collected in two ways: (i) during wetting, by infiltration of metal solutions through the cellulosic film (Figure S8), and (ii) drying of the already wet film (Figure 4e–g). The data for the dry sample ($t = 0$) were modeled by using the generalized Debye–Anderson–Brumberger (gDAB) model. As the time increases and the metal ion solution passes through, the SAXS data show an evolution of the scattering buildup in the intermediate Q range (Figure S8). The data in this set have been analyzed by combining the gDAB equation (eq 5), accounting for the scattering contributions from the film at low Q values with a form factor (eq 2) of the polydisperse spheres, to account for the scattering buildup at the intermediate Q values. The analyses suggest the formation of nanoparticles in the size range of about 4–6 nm with a polydispersity (σ) of about 0.2–0.3 in the log-normal distribution.

Nevertheless, the actual growth of the NPS is indeed observed during drying of the films. The in-situ SAXS data [$I(Q)$ vs Q vs time] during the drying of the films are presented in Figure 4e–g. The SAXS spectra clearly show the scattering buildup, extended up to the low Q region, with typical features of the form factor governed scattering (Figure 4e). Some of the data collected at different times (Figure 4f) are also presented by plotting $I(Q)$ vs Q which shows the narrowing width of the scattering profile, suggesting the growth of the NPS. The entire data set in this case were also fitted by combining the contributions from wet cellulose film and NPS. The variation of the diameters with time is shown in the Figure 4g, which is found to be in the range of about 10–20 nm, consistent with the observations of the AFM (Figure 2a).

Applications of Cu_2O/TOCNF Films. We studied the functionality of the resultant Cu_2O/TOCNF hybrid films, after adsorption of Cu^{2+} ions and subsequent formation of Cu_2O-

https://dx.doi.org/10.1021/acsanm.0c01511
ACS Appl. Nano Mater. 2020, 3, 7172–7181

NPS. The removal of dyes from aqueous solutions and antimicrobial activity were chosen as the properties to evaluate the performance and potential applications of the hybrid films. The results are described as follows.

Dye Removal from Aqueous Solutions. The capacity of the Cu_2O/TOCNF hybrid films to remove dyes from aqueous solutions was studied under UV-light irradiation (MB was used as model system), considering that Cu_2O-NPS exhibit the capacity to synergistically adsorb and photocatalyze the degradation of dyes.[40−42] The results, shown in Figure 5a,b,

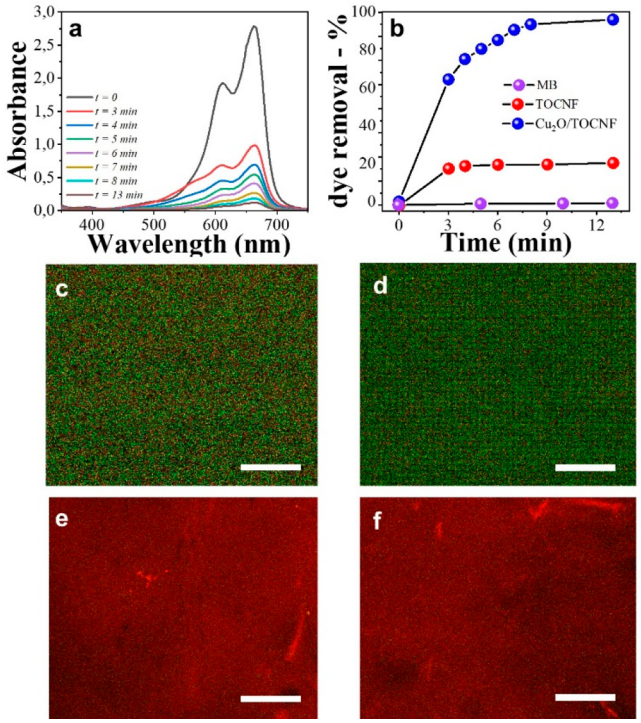

Figure 5. Applications of Cu_2O/TOCNF films. (a) UV−vis spectra of MB in the presence of hybrid film under irradiation of direct UV light. (b) Dye removal (%) of MB [20 ppm] during direct UV-light irradiation. (c−f) Antibacterial properties of films: (c) TOCNF film inoculated with *E. coli* and (d) *L. innocua*. (e) Cu_2O/TOCNF hybrid film inoculated with *E. coli* and (f) *L. innocua*. Live cells are shown in green, and dead cells are shown in red. Scale bar = 100 μm.

show the dye removal (%) as a function of time, proving how almost all MB disappeared from the aqueous solution after 8 min in the presence of the Cu_2O/TOCNF (Figures S9 and S10); indeed, the Cu_2O-NPS increased the dye removal capacity to nearly 60% (Figure 5b) compared to pure TOCNF. As previously mentioned, the high efficiency of Cu_2O-NPS to remove dyes arises from the combination of both adsorptive capacity and UV-light-mediated degradation acting synergistically. The general mechanism of the photocatalyzed dye degradation by Cu_2O-NPS is briefly described as follows: when irradiated by light with photo energy greater than the band gap, electrons of the Cu_2O-NPS are promoted to the conduction band, creating holes in the valence band. Electrons in the conduction band can then react with molecular oxygen to produce intermediate superoxide ($O_2^{\bullet-}$) radicals, which then act as a precursor for H_2O_2 and ($^{\bullet}OH$) radicals (a strong and nonselective oxidant). These species are the main reactive species for the photocatalyzed dye degradation.[41−44]

Antibacterial Properties. The antibacterial properties of Cu_2O/TOCNF films were studied with common Gram-negative (*E. coli*) and Gram-positive (*L. innocua*) bacteria. It is known that Cu_2O-NPS exhibit excellent antibacterial properties, presumably due to the disruption of biochemical processes inside the bacterial cells or via binding with DNA molecules that leads to disorder of the helical structure by cross-linking within and between the nucleic acid strands.[45−47] As shown in Figure 5c−f, the number of dead cells (in red) far outweighs the number of live cells (in green) for Cu_2O/TOCNF hybrid films, and no significant difference was observed between Gram-positive and Gram-negative bacteria. This clearly shows that the presence of Cu_2O-NPS confers the films strong antibacterial activity against both classes of bacteria. This antimicrobial effect was observed even at low metal ion concentrations (Figure S11), proving the robustness of this method to synthesize biocidal materials against a wide range of bacteria. On the other hand, TOCNF is known to be an excellent candidate for water purification, and therefore its hybridization with Cu_2O-NPS can take the applicability of these films for water purification up to next level by combining the suitable features of the nanocellulose and antibacterial properties of the Cu_2O-NPS.

The outstanding dye-removal capacity and antimicrobial properties of Cu_2O/TOCNF suggest the possible multistage employment of these nanocellulose-based materials, upon acquisition of new properties during the purification of aqueous solutions from metal ions, besides increasing the value in terms of sustainability for carboxylated nanocellulose. In other words, our results suggest the possibility to use TOCNF not only to purify heavy metal ions from water but also to subsequently provide functionality which can be used to remove dyes and kill microorganisms. Such a versatile and energy-efficient way to introduce functionality to bio-based materials establishes a strong sustainable pathway that can be extended toward different applications.

Universal Growth of MO-NPS. The universal capacity of TOCNF to grow other MO-NPS was demonstrated by carrying out similar studies with silver nitrate (Figure 6 and Figure S12) and iron(III) nitrate salts (Figure S13), submerging TOCNF films in the corresponding salt solutions at 800 mg L^{-1} for 60 min and drying overnight at room temperature. All the experimental conditions to grow silver and iron oxide nanoparticles were kept the same as that used for Cu_2O. The UV−vis spectra (Figure 6a) show a clear evolution in the absorbance as a function of time in wavelengths around 240 nm, assimilating to the case of Cu_2O-NPS. For the silver salt solution, XPS revealed the formation of silver oxide (Ag_2O) nanoparticles (SONPS) on TOCNF, as the resultant Ag 3d spectra exhibit the two typical peaks located at ≈368 and 375 eV (Figure 6b), corresponding to Ag $3d_{5/2}$ and Ag $3d_{3/2}$ bonding energies,[48] respectively. Upon deconvolution of each Ag 3d level, two peaks were revealed for Ag $3d_{5/2}$ with binding energies of ≈367.5 and 368.8 eV, corresponding to AgO and Ag_2O,[49] respectively (Ag^+/Ag^{2+} integral area ratio ≈5). This behavior presumably occurs due to the a disproportionation reaction that occurs at the surface of Ag_2O, as it has been previously reported.[50] Further XPS information is given in the Supporting Information (Figure S12, S13 and Tables S2, S3). The in-situ SAXS data while adsorption (Figure S8b,d) of the Ag^+ ions on nanocellulose film (wetting of film) and during afterward drying (Figure 6c) of the film also revealed the formation of the nanoclusters and nanoparticles. The data show similar features as observed and discussed in the case of Cu_2O/TOCNF. In this case also, the actual growth of the

https://dx.doi.org/10.1021/acsanm.0c01511
ACS Appl. Nano Mater. 2020, 3, 7172−7181

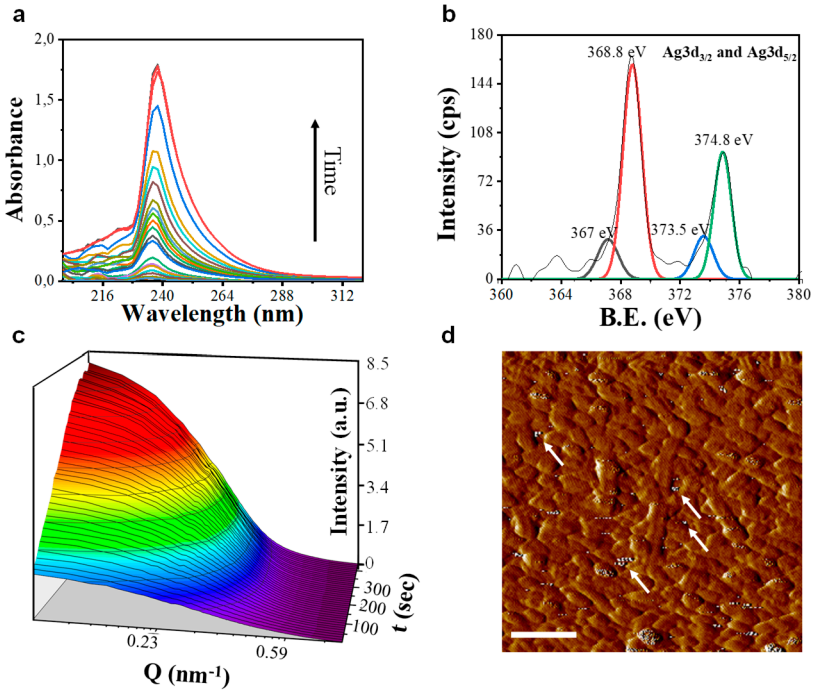

Figure 6. In-situ growth of Ag_2O/TOCNF. (a) UV−vis spectra of TOCNF-hybrid films tracking the formation of Ag_2O nanoclusters. (b) High-resolution Ag 3d XPS spectra of Ag_2O/TOCNF-hybrid films. (c) Three-dimensional SAXS plots [$I(Q)$ vs Q vs time] during drying of nanocellulose films after copper adsorption. (d) AFM micrograph of Ag_2O/TOCNF (scale bar = 200 nm).

SONPS occurs during drying of the films, where the SAXS spectra clearly show the evolution of scattering buildup, depicting the typical features of the form factor governed scattering. The scattering data were analyzed in the same manner as described for the Cu_2O/TOCNF system, and the obtained nanoparticle sizes as a function of time are shown in Figure S14. Furthermore, the SONPS were also visualized in AFM (Figure 6d). The relevant results for the iron(III) nitrate salts are provided in Figure S15.

CONCLUSIONS

In this work, we systematically demonstrate the capacity of carboxylated cellulose nanofibril films to spontaneously form MO-NPS occurring in situ during the adsorption of metal ions from aqueous solution, without the use of any chemical or temperature increase. The growth of Cu_2O-NPS provides important functionality to the nanocellulosic films, for instance, antimicrobial properties and enhancement in the capacity to remove dyes from aqueous solutions, proving to be a green alternative toward the preparation of multifunctional hybrid materials. By studying the nanoparticle formation in situ through a combination of synchrotron-based SAXS, QCMD, and UV−vis spectroscopy, we proposed a possible mechanism of assembly, which agrees with the growth and coalescence model. Our results suggest a multistage employment of nanocellulose-based materials to prepare hybrids materials during the filtration of metal ions solution.

ASSOCIATED CONTENT

Supporting Information

The Supporting Information is available free of charge at https://pubs.acs.org/doi/10.1021/acsanm.0c01511.

Further characterization of materials including X-ray diffraction (XRD), X-ray photoelectron spectroscopy (XPS), atomic force microscopy (AFM), scanning electron microscopy (SEM), and ultraviolet spectroscopy (UV−vis); data regarding Ag_2O/TOCNF and Fe_2O_3/TOCNF (PDF)

AUTHOR INFORMATION

Corresponding Authors

Aji P. Mathew − *Department of Materials and Environmental Chemistry, Stockholm University, 10691 Stockholm, Sweden;* orcid.org/0000-0001-8909-3554; Email: aji.mathew@mmk.su.se

Luis Valencia − *Department of Materials and Environmental Chemistry, Stockholm University, 10691 Stockholm, Sweden; Materials Technology and Chemistry, SE-14782 Tumba, Sweden;* orcid.org/0000-0001-6572-7460; Email: luisalex_val@hotmail.com

Authors

Sugam Kumar − *Department of Materials and Environmental Chemistry, Stockholm University, 10691 Stockholm, Sweden; Solid State Physics Division, Bhabha Atomic Research Centre, Mumbai 400 085, India*

Emma M. Nomena − *Unilever Foods Innovation Centre, 6708 WH Wageningen, The Netherlands; Institute of Physics, University of Amsterdam, 1098 XH Amsterdam, The Netherlands;* orcid.org/0000-0003-0304-9865

German Salazar-Alvarez − *Department of Materials and Environmental Chemistry, Stockholm University, 10691 Stockholm, Sweden;* orcid.org/0000-0002-0671-435X

Complete contact information is available at: https://pubs.acs.org/10.1021/acsanm.0c01511

Author Contributions

L.V. and S.K. contributed equally to this work.

https://dx.doi.org/10.1021/acsanm.0c01511
ACS Appl. Nano Mater. 2020, 3, 7172−7181

Notes

The authors declare no competing financial interest.

■ ACKNOWLEDGMENTS

The authors acknowledge the MULTIMAT project (H2020-MSCA-ITN-2014, Grant No. 676045) and the Swedish Research Council (VR, Grant No. 2017-04254) for research funding. The authors also thank DESY, Hamburg, Germany, for the beamtime I-20170358 and beamline scientist Dr. Wiebke Ohm for her support during the experiments. Dr. Peng Liu, SU, is acknowledged for the support during the in-situ SAXS experiments.

■ REFERENCES

(1) Pouget, E.; Dujardin, E.; Cavalier, A.; Moreac, A.; Valéry, C.; Marchi-Artzner, V.; Weiss, T.; Renault, A.; Paternostre, M.; Artzner, F. Hierarchical Architectures by Synergy between Dynamical Template Self-Assembly and Biomineralization. *Nat. Mater.* **2007**, *6* (6), 434−439.

(2) Valencia, L.; Rosas-Arbelaez, W.; Aguilar-Sánchez, A.; Mathew, A. P.; Palmqvist, A. E. C. Biobased Micro/Meso/Macro-Porous Hybrid Foams with Ultra-High Zeolite Loadings for Selective Capture of Carbon Dioxide. *ACS Appl. Mater. Interfaces* **2019**, *11* (43), 40424−40431.

(3) Thomas, B.; Raj, M. C.; B, A. K.; H, R. M.; Joy, J.; Moores, A.; Drisko, G. L.; Sanchez, C. Nanocellulose, a Versatile Green Platform: From Biosources to Materials and Their Applications. *Chem. Rev.* **2018**, *118* (24), 11575−11625.

(4) Lagerwall, J. P. F.; Schütz, C.; Salajkova, M.; Noh, J.; Hyun Park, J.; Scalia, G.; Bergström, L. Cellulose Nanocrystal-Based Materials: From Liquid Crystal Self-Assembly and Glass Formation to Multifunctional Thin Films. *NPG Asia Mater.* **2014**, *6* (1), No. e80.

(5) Frka-Petesic, B.; Vignolini, S. So Much More than Paper. *Nat. Photonics* **2019**, *13* (6), 365−367.

(6) Valencia, L.; Arumughan, V.; Jalvo, B.; Maria, H. J.; Thomas, S.; Mathew, A. P. Nanolignocellulose Extracted from Environmentally Undesired. *Prosopis Juliflora. ACS Omega* **2019**, *4* (2), 4330−4338.

(7) Valencia, L.; Kumar, S.; Jalvo, B.; Mautner, A.; Salazar-Alvarez, G.; Mathew, A. P. Fully Bio-Based Zwitterionic Membranes with Superior Antifouling and Antibacterial Properties Prepared via Surface-Initiated Free-Radical Polymerization of Poly(Cysteine Methacrylate). *J. Mater. Chem. A* **2018**, *6* (34), 16361−16370.

(8) Valencia, L.; Abdelhamid, H. N. Nanocellulose Leaf-like Zeolitic Imidazolate Framework (ZIF-L) Foams for Selective Capture of Carbon Dioxide. *Carbohydr. Polym.* **2019**, *213* (2), 338−345.

(9) Padalkar, S.; Capadona, J. R.; Rowan, S. J.; Weder, C.; Won, Y. H.; Stanciu, L. A.; Moon, R. J. Natural Biopolymers: Novel Templates for the Synthesis of Nanostructures. *Langmuir* **2010**, *26* (11), 8497−8502.

(10) Schütz, C.; Sort, J.; Bacsik, Z.; Oliynyk, V.; Pellicer, E.; Fall, A.; Wågberg, L.; Berglund, L.; Bergström, L.; Salazar-Alvarez, G. Hard and Transparent Films Formed by Nanocellulose-TiO_2 Nanoparticle Hybrids. *PLoS One* **2012**, *7* (10), 1−8.

(11) Rezayat, M.; Blundell, R. K.; Camp, J. E.; Walsh, D. A.; Thielemans, W. Green One-Step Synthesis of Catalytically Active Palladium Nanoparticles Supported on Cellulose Nanocrystals. *ACS Sustainable Chem. Eng.* **2014**, *2* (5), 1241−1250.

(12) Kaushik, M.; Moores, A. Review: Nanocelluloses as Versatile Supports for Metal Nanoparticles and Their Applications in Catalysis. *Green Chem.* **2016**, *18* (3), 622−637.

(13) Eisa, W. H.; Abdelgawad, A. M.; Rojas, O. J. Solid-State Synthesis of Metal Nanoparticles Supported on Cellulose Nanocrystals and Their Catalytic Activity. *ACS Sustainable Chem. Eng.* **2018**, *6* (3), 3974−3983.

(14) Olsson, R. T.; Azizi Samir, M. a S.; Salazar-Alvarez, G.; Belova, L.; Ström, V.; Berglund, L. A.; Ikkala, O.; Nogués, J.; Gedde, U. W. Making Flexible Magnetic Aerogels and Stiff Magnetic Nanopaper Using Cellulose Nanofibrils as Templates. *Nat. Nanotechnol.* **2010**, *5* (8), 584−588.

(15) Le, D.; Kongparakul, S.; Samart, C.; Phanthong, P.; Karnjanakom, S.; Abudula, A.; Guan, G. Preparing Hydrophobic Nanocellulose-Silica Film by a Facile One-Pot Method. *Carbohydr. Polym.* **2016**, *153* (20), 266−274.

(16) Zheng, Q.; Cai, Z.; Ma, Z.; Gong, S. Cellulose Nanofibril/Reduced Graphene Oxide/Carbon Nanotube Hybrid Aerogels for Highly Flexible and All-Solid-State Supercapacitors. *ACS Appl. Mater. Interfaces* **2015**, *7* (5), 3263−3271.

(17) Yoo, Y.; Youngblood, J. P. Green One-Pot Synthesis of Surface Hydrophobized Cellulose Nanocrystals in Aqueous Medium. *ACS Sustainable Chem. Eng.* **2016**, *4* (7), 3927−3938.

(18) Ma, H.; Hsiao, B. S.; Chu, B. Ultrafine Cellulose Nanofibers as Efficient Adsorbents for Removal of UO22+ in Water. *ACS Macro Lett.* **2012**, *1* (1), 213−216.

(19) Isogai, A.; Saito, T.; Fukuzumi, H. TEMPO-Oxidized Cellulose Nanofibers. *Nanoscale* **2011**, *3* (1), 71−85.

(20) Voisin, H.; Bergström, L.; Liu, P.; Mathew, A. Nanocellulose-Based Materials for Water Purification. *Nanomaterials* **2017**, *7* (3), 57.

(21) Saito, T.; Isogai, A. Ion-Exchange Behavior of Carboxylate Groups in Fibrous Cellulose Oxidized by the TEMPO-Mediated System. *Carbohydr. Polym.* **2005**, *61* (2), 183−190.

(22) Sehaqui, H.; de Larraya, U. P.; Liu, P.; Pfenninger, N.; Mathew, A. P.; Zimmermann, T.; Tingaut, P. Enhancing Adsorption of Heavy Metal Ions onto Biobased Nanofibers from Waste Pulp Residues for Application in Wastewater Treatment. *Cellulose* **2014**, *21* (4), 2831−2844.

(23) Zhu, C.; Soldatov, A.; Mathew, A. P. Advanced Microscopy and Spectroscopy Reveal the Adsorption and Clustering of Cu(II) onto TEMPO-Oxidized Cellulose Nanofibers. *Nanoscale* **2017**, *9* (22), 7419−7428.

(24) Liu, P.; Oksman, K.; Mathew, A. P. Surface Adsorption and Self-Assembly of Cu(II) Ions on TEMPO-Oxidized Cellulose Nanofibers in Aqueous Media. *J. Colloid Interface Sci.* **2016**, *464*, 175−182.

(25) Zhu, C.; Monti, S.; Mathew, A. P. Cellulose Nanofiber-Graphene Oxide Biohybrids: Disclosing the Self-Assembly and Copper-Ion Adsorption Using Advanced Microscopy and ReaxFF Simulations. *ACS Nano* **2018**, *12* (7), 7028−7038.

(26) Saito, T.; Isogai, A. TEMPO-Mediated Oxidation of Native Cellulose. The Effect of Oxidation Conditions on Chemical and Crystal Structures of the Water-Insoluble Fractions. *Biomacromolecules* **2004**, *5* (5), 1983−1989.

(27) Tellechea, E.; Johannsmann, D.; Steinmetz, N. F.; Richter, R. P.; Reviakine, I. Model-Independent Analysis of QCM Data on Colloidal Particle Adsorption. *Langmuir* **2009**, *25* (9), 5177−5184.

(28) Salavati-Niasari, M.; Davar, F. Synthesis of Copper and Copper(I) Oxide Nanoparticles by Thermal Decomposition of a New Precursor. *Mater. Lett.* **2009**, *63* (3), 441−443.

(29) Oh, S. Y.; Yoo, D. Il; Shin, Y.; Kim, H. C.; Kim, H. Y.; Chung, Y. S.; Park, W. H.; Youk, J. H. Crystalline Structure Analysis of Cellulose Treated with Sodium Hydroxide and Carbon Dioxide by Means of X-Ray Diffraction and FTIR Spectroscopy. *Carbohydr. Res.* **2005**, *340* (15), 2376−2391.

(30) Yao, W. T.; Yu, S. H.; Zhou, Y.; Jiang, J.; Wu, Q. S.; Zhang, L.; Jiang, J. Formation of Uniform CuO Nanorods by Spontaneous Aggregation: Selective Synthesis of CuO, Cu_2O, and Cu Nanoparticles by a Solid-Liquid Phase Arc Discharge Process. *J. Phys. Chem. B* **2005**, *109* (29), 14011−14016.

(31) Valencia, L.; Nomena, E. M.; Monti, S.; Rosas-Arbelaez, W.; Mathew, A. P.; Kumar, S.; Velikov, K. P. Multivalent Ion-Induced Re-Entrant Transition of Carboxylated Cellulose Nanofibrils and Its Influence on Nanomaterials Properties. *Nanoscale* **2020**, DOI: 10.1039/D0NR02888F.

(32) Dong, H.; Snyder, J. F.; Williams, K. S.; Andzelm, J. W. Cation-Induced Hydrogels of Cellulose Nanofibrils with Tunable Moduli. *Biomacromolecules* **2013**, *14* (9), 3338−3345.

(33) Batool, F.; Akbar, J.; Iqbal, S.; Noreen, S.; Nasir, S.; Bukhari, A. Study of Isothermal, Kinetic, and Thermodynamic Parameters for Adsorption of Cadmium: An Overview of Linear and Nonlinear Approach and Error Analysis. *Bioinorg. Chem. Appl.* **2018**, *2018*, 1−11.

https://dx.doi.org/10.1021/acsanm.0c01511
ACS Appl. Nano Mater. 2020, 3, 7172−7181

(34) Liu, P.; Oksman, K.; Mathew, A. P. Surface Adsorption and Self-Assembly of Cu(II) Ions on TEMPO-Oxidized Cellulose Nanofibers in Aqueous Media. *J. Colloid Interface Sci.* **2016**, *464*, 175−182.
(35) Liu, J.; Wang, X. Novel Silica-Based Hybrid Adsorbents: Lead (II) Adsorption Isotherms Novel Silica-Based Hybrid Adsorbents: Lead (II) Adsorption Isotherms. *Sci. World J.* **2013**, *2013*, 1.
(36) Ranaivoarimanana, N. J.; Kanomata, K.; Kitaoka, T. Concerted Catalysis by Nanocellulose and Proline in Organocatalytic Michael Additions. *Molecules* **2019**, *24* (7), 1231.
(37) Kanomata, K.; Tatebayashi, N.; Habaki, X.; Kitaoka, T. Cooperative Catalysis of Cellulose Nanofiber and Organocatalyst in Direct Aldol Reactions. *Sci. Rep.* **2018**, *8* (1), 6−10.
(38) Polte, J. Fundamental Growth Principles of Colloidal Metal Nanoparticles - a New Perspective. *CrystEngComm* **2015**, *17* (36), 6809−6830.
(39) Valencia, L.; Monti, S.; Kumar, S.; Liu, P.; Zhu, C.; Yu, S.; Mathew, A. Nanocellulose/Graphene Oxide Layered Membranes: Elucidating Their Behaviour during Filtration of Water and Metal Ions in Real Time. *Nanoscale* **2019**, *11*, 22413−22422.
(40) Shu, J.; Wang, Z.; Huang, Y.; Huang, N.; Ren, C.; Zhang, W. Adsorption Removal of Congo Red from Aqueous Solution by Polyhedral Cu_2O Nanoparticles: Kinetics, Isotherms, Thermodynamics and Mechanism Analysis. *J. Alloys Compd.* **2015**, *633* (5), 338−346.
(41) Fageria, P.; Gangopadhyay, S.; Pande, S. Synthesis of ZnO/Au and ZnO/Ag Nanoparticles and Their Photocatalytic Application Using UV and Visible Light. *RSC Adv.* **2014**, *4* (48), 24962−24972.
(42) Zheng, Y.; Zheng, L.; Zhan, Y.; Lin, X.; Zheng, Q.; Wei, K. Ag/ZnO Heterostructure Nanocrystals: Synthesis, Characterization, and Photocatalysis. *Inorg. Chem.* **2007**, *46* (17), 6980−6986.
(43) Pal, J.; Ganguly, M.; Mondal, C.; Roy, A.; Negishi, Y.; Pal, T. Crystal-Plane-Dependent Etching of Cuprous Oxide Nanoparticles of Varied Shapes and Their Application in Visible Light Photocatalysis. *J. Phys. Chem. C* **2013**, *117* (46), 24640−24653.
(44) Xiong, L.; Xiao, H.; Chen, S.; Chen, Z.; Yi, X.; Wen, S.; Zheng, G.; Ding, Y.; Yu, H. Fast and Simplified Synthesis of Cuprous Oxide Nanoparticles: Annealing Studies and Photocatalytic Activity. *RSC Adv.* **2014**, *4* (107), 62115−62122.
(45) Abboud, Y.; Saffaj, T.; Chagraoui, A.; El Bouari, A.; Brouzi, K.; Tanane, O.; Ihssane, B. Biosynthesis, Characterization and Antimicrobial Activity of Copper Oxide Nanoparticles (CONPs) Produced Using Brown Alga Extract (Bifurcaria Bifurcata). *Appl. Nanosci.* **2014**, *4* (5), 571−576.
(46) Kim, J. H.; Cho, H.; Ryu, S. E.; Choi, M. U. Effects of Metal Ions on the Activity of Protein Tyrosine Phosphatase VHR: Highly Potent and Reversible Oxidative Inactivation by Cu2+ Ion. *Arch. Biochem. Biophys.* **2000**, *382* (1), 72−80.
(47) Stohs, S. J.; Bagchi, D. Oxidative Mechanisms in the Toxicity of Metal Ions. *Free Radical Biol. Med.* **1995**, *18* (2), 321−336.
(48) Wei, N.; Cui, H.; Song, Q.; Zhang, L.; Song, X.; Wang, K.; Zhang, Y.; Li, J.; Wen, J.; Tian, J. Ag2O Nanoparticle/TiO_2nanobelt Heterostructures with Remarkable Photo-Response and Photocatalytic Properties under UV, Visible and near-Infrared Irradiation. *Appl. Catal., B* **2016**, *198*, 83−90.
(49) Wei, W.; Mao, X.; Ortiz, L. A.; Sadoway, D. R. Oriented Silver Oxide Nanostructures Synthesized through a Template-Free Electrochemical Route. *J. Mater. Chem.* **2011**, *21* (2), 432−438.
(50) Hoflund, G. B.; Hazos, Z. F.; Salaita, G. N. Surface Characterization Study of Ag, AgO, and Ag2O Using x-Ray Photoelectron Spectroscopy and Electron Energy-Loss Spectroscopy. *Phys. Rev. B: Condens. Matter Mater. Phys.* **2000**, *62* (16), 11126−11133.

https://dx.doi.org/10.1021/acsanm.0c01511
ACS Appl. Nano Mater. 2020, 3, 7172−7181